Texturing of hydrothermally synthesized $BaTiO_3$ in a strong magnetic field by slip casting

Texturing of hydrothermally synthesized $BaTiO_3$ in a strong magnetic field by slip casting

Murat Özen, Myrjam Mertens, Frans Snijkers, Gustaaf Van Tendeloo, Pegie Cool

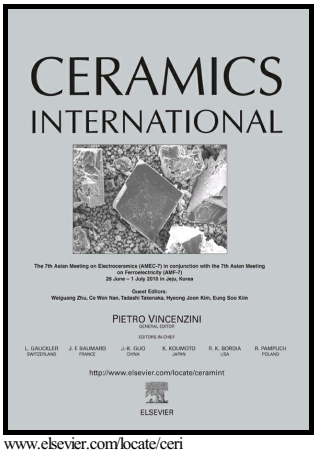

www.elsevier.com/locate/ceri

PII: S0272-8842(15)02371-8
DOI: http://dx.doi.org/10.1016/j.ceramint.2015.12.073
Reference: CERI11868

To appear in: *Ceramics International*

Received date: 11 November 2015
Revised date: 28 November 2015
Accepted date: 16 December 2015

Cite this article as: Murat Özen, Myrjam Mertens, Frans Snijkers, Gustaaf Van Tendeloo and Pegie Cool, Texturing of hydrothermally synthesized $BaTiO_3$ in a strong magnetic field by slip casting, *Ceramics International*, http://dx.doi.org/10.1016/j.ceramint.2015.12.073

Texturing of hydrothermally synthesized $BaTiO_3$ in a strong magnetic field by slip casting

Murat Özen[a,*], Myrjam Mertens[b], Frans Snijkers[b], Gustaaf Van Tendeloo[c], Pegie Cool[a]

[a]Laboratory of Adsorption and Catalysis, Department of Chemistry, University of Antwerp, Universiteitsplein 1, B-2610 Wilrijk, Belgium

*Corresponding author. Email address: murat.ozen@outlook.com T +32 3 265 2380 F +32 3 265 2374

[b]Flemish Institute for Technology Research (VITO nv), Boeretang 200, B-2400 Mol, Belgium

[c]EMAT, University of Antwerp, Groenenborgerlaan 171, B-2020 Antwerpen, Belgium

Abstract

Barium titanate powder was processed by slip casting in a rotating strong magnetic field of 9.4 tesla. The orientation factor of the sintered compact was analyzed by the X-ray diffraction technique and the microstructure (grain-size) was analyzed by scanning electron microscope. The hydrothermally prepared barium titanate was used as matrix material and the molten-salt synthesized barium titanate, with a larger particle-size, was used as template for the templated grain-growth process. Addition of large template particles was observed to increase the orientation factor of the sintered cast (5 vol% loading). Template particles acted as starting grains for the abnormal grain-growth process and the average grain-size was increased after sintering. Increasing the solid loading (15 vol%) resulted in a similar orientation factor with a decrease of the average grain-size by more than half. However, addition of templates to the 15 vol% cast had a negative effect on the orientation factor. The impingement of growing particles was stated as the primary cause of particle misorientation resulting in a low orientation factor after sintering. Different heating conditions were tested and it was determined that a slow heating rate gave the highest orientation factor, the smallest average grain-size and the highest relative density.

Keywords: A. Slip casting, B. X-ray methods, D. $BaTiO_3$, Magnetic alignment

1. Introduction

The properties of materials can be enhanced by texturing. There are several techniques to accomplish this. Texturing of ceramic materials by colloidal processing is one of these techniques. Colloidal processing has been extensively investigated for net shaping methods such as gel casting[1–3], electrophoretic deposition[4,5] and slip casting[4,6–9]. Controlled conditions of the starting powder, slurry preparation, organic additive removal and sintering resulted in high-quality dense ceramic materials for industrial, medical and commercial use. Colloidal processing by means of the templated grain-growth method (TGG)[8,10,11] is another inventive technique to align ceramic particles. In the TGG method, a fraction of the particles consists of large single-crystals with defined crystallographic habit planes. During processing of the colloidal dispersion and subsequent sintering the template grains grow and consume the matrix grains to produce a textured microstructure.

Texture of ceramic materials with interesting properties in a strong magnetic field has gained much attention recently.[2,3,5,8,9,12] The very low diamagnetic susceptibilities (χ) of ceramic materials did not make them very attractive for magnetic studies. However, the development of magnets with strong fields by the use of superconducting materials made the study of feeble diamagnetic ceramics much more appealing.[1,13–15]

Particle alignment in a magnetic field is governed by various factors. These factors are expressed in the following equation:

$$|\Delta E| = \frac{|\Delta\chi|\, V\, B^2}{2\,\mu_0} \qquad (1)$$

with V the volume of the ceramic particle, B the magnetic flux density or, simply, the magnetic field, $\Delta\chi$ the anisotropy in diamagnetic susceptibilities, μ_0 the permeability of free space and $|\Delta E|$ the magnetization energy.[6]

Barium titanate ($BaTiO_3$) is the most widely investigated perovskite material due to its piezoelectric and ferroelectric properties.[14,16,17] Various synthesis methods were developed for perovskite-type materials over the years. The molten-salt method offers several advantages such as: a relatively low crystallization temperature, a better homogeneity, and a better morphology control of the end-product. Basically, a molten-

salt synthesis (MSS) reaction consists of stoichiometric mixture of the oxide and equal amount of the salt which are heated above the melting point of the salt. At this point the salt is in its liquid state and acts as a reaction medium to facilitate the reaction between the oxides. Homogeneous powders with controllable particle size and morphology are one of the advantages of MSS.[18–21] It is believed that the features obtained by the molten-salt technique are related to the surface and interface energies between the constituents and the salt, resulting in a tendency to minimize the energies by forming a specific morphology.[22]

The hydrothermal process is an effective method due to its attractive processing feature of low temperature processing.[23] However, the control of particle morphology in solution synthesis is a complex process. A fundamental understanding of the interactions between solid state chemistry, interfacial reactions and kinetics, and solution chemistry is required. Parameters which affect super saturation conditions, hence particle morphology, are solution pH, temperature, precursor concentration, and agitation.[24,25]

Little is known about the diamagnetic susceptibility axes of $BaTiO_3$. The tetragonal crystal phase has a very low crystallographic anisotropy which can be derived from the low c:a ratio (~1.007). This in turn is reflected in a very low anisotropy in diamagnetic susceptibility. It is assumed that the c-axis of $BaTiO_3$ is the easy magnetization axis ($\chi_c < \chi_{a,b} < 0$). Since, $BaTiO_3$ is diamagnetic in nature the easy magnetization axis will turn away from the magnetic field direction to minimize its energy. Hence, the c-axis is expected to align perpendicular to the magnetic field B. However, this was not confirmed by literature. In fact, very few literature is available on textured perovskite ceramics in general and barium titanate in specific.[1,4–6] The available literature mainly reports on [111] & [101]- or [101]-textured $BaTiO_3$.[1,5] Publications on textured $BaTiO_3$ are limited and reports of highly textured $BaTiO_3$ are even scarcer. Özen et al.[6] investigated the grain alignment of hydrothermally prepared $BaTiO_3$ by slip casting in a 9.4 T magnetic field. They reported the aligment of {001} planes normal to the magnetic field with an orientation factor of 0.25 for the as-sintered samples. Wada et al.[5] performed slip casting of nano-sized $BaTiO_3$ in a magnetic field of 12 T. They obtained a strong alignment along the [111] direction for the as-sintered slip casts. However, after polishing of the as-sintered slip casts the $BaTiO_3$ ceramics were reported to be randomly oriented. Vriami et al.[4] reported the texture of hydrothermally synthesized $BaTiO_3$ in a very strong magnetic field of 17.4 T by slip

casting with an orientation factor of 0.67 for samples sintered at 1450°C. The $BaTiO_3$ ceramics were reported to have a fiber texture with the <001> fiber axis aligning parallel to the direction of the magnetic field. Another important factor is the sintering temperature. Sintering (> 1000°C) is applied to densify and increase texture of the material. However, barium titanate will be sintered in the cubic form at elevated temperatures, up to 1420°C to be exactly.[26] The tetragonal form will reappear upon cooling. The question then arises whether the material will keep its original orientation.

The slip casting of $BaTiO_3$ inside a 9.4 tesla (T) magnet for the purpose of alignment will be studied here. The hydrothermally prepared $BaTiO_3$ was subjected to the high magnetic field by slip casting whereby the molten-salt prepared $BaTiO_3$ was used as template particles. The orientation factor f, the microstructure and the densities of the sintered casts were studied as a function of different heating temperatures and heating conditions.

2. Material and methods

2.1. Synthesis of the barium-titanium-peroxo-hydroxide precursor

A barium-titanium precursor was produced first by the peroxo-hydroxide method.[27] The barium reagent was added to demineralized water and $TiCl_4$ (99.9%, Acros) was added to the barium solution with a syringe, to minimize contact with air, under vigorous stirring so that the dissolution of $TiCl_4$ proceeded in a minimum amount of time. The barium and titanium concentrations were adjusted so that the barium to titanium ratio amounted to 2. The total barium and titanium concentration was fixed at 0.05 M. Immediately after having added $TiCl_4$ to the barium solution, hydrogen peroxide (H_2O_2, 35%, Acros) was added dropwise to the solution (pH = 1.2). The H_2O_2 to titanium ratio was fixed at 3. The complexation reaction was visible by the formation of a clear dark red colored solution.[28] The excess hydrogen peroxide ensures the deprotonation of the titanium hydroxo-aquo complex. The overall reaction is given by eq.(2) (water molecules are not shown):

$$Ba^{2+}_{(aq),excess} + 2\,Ti(OH)_2^{2+}{}_{(aq)} + H_2O_{2\,(aq),excess} \rightleftharpoons Ba^{2+}_{(aq),excess} + 2\,Ti(O)_2(OH)_{N-2}^{4-N+}{}_{(aq)} + N\,H^+_{(aq)} \quad (2)$$

where N denotes the number of hydrogen ions which are liberated from the titanium-aquo ion.

The solution was then stirred for an additional 30 minutes. Coprecipitation of metal-hydroxides in aqueous solutions is initiated by solubility change depending on pH.[29] Therefore, the precursor solution was precipitated by the dropwise addition of NH_4OH (28-30%, Acros) till pH 10.1 ± 0.2 which was accompanied by a color change of the suspension from dark red to non-transparent milky pale green. By the addition of the alkaline reagent a polymerization reaction was initiated which resulted in the cross-linked network of $Ti-O-Ti$ bonds with Ba^{2+} ions located in the 'cavities' of the cross-linked structure. The overall reaction is shown in eq.(3):[28]

$$(pH > 9): \quad Ba^{2+}_{(aq),excess} + Ti_2O_5(OH)_6^{4-}{}_{(aq)} \rightleftharpoons Ba_2Ti_2O_5(OH)_{6\,(s)} \quad (3)$$

The barium-titanium-peroxo-hydroxide complex solution was stirred for 2 h (hours). Afterwards, the metal coprecipitate was filtrated with a Buchner funnel and washed three times with demineralized water. The coprecipitate was then dried overnight at room temperature and crushed to fine powder with a ceramic mortar.

2.2. Hydrothermal $BaTiO_3$ synthesis

Hydrothermal reactions were conducted in a stainless steel reactor from Berghof (Germany). The barium-titanium precursor was hydrothermally treated in a 10 M NaOH solution at 200°C for 24 h. The hydrothermal product was washed with demineralized water and dried overnight at room temperature. Afterwards, the powder was ball milled and freeze dried in order to break agglomerates and heated at 950°C for 1 h to eliminate hydroxyl groups from the oxygen sub-lattice.[30] The median particle-size of the hydrothermally prepared $BaTiO_3$ powder was 0.48 µm (see Fig. 1a).

2.3. Molten-salt synthesis of $BaTiO_3$

Eutectic salt mixtures were reported such as $NaCl-KCl$, $Na_2SO_4-K_2SO_4$, $NaOH-KOH$, $LiCl-KCl$ and

$BaCl_2 - KCl$.[10,18,19,21,31–37] In the case of Li-based salt systems mixed phases and even unreacted reagents were found. Hydroxide ions, in a $NaOH - KOH$ flux for example, were said to be actively participating in the reaction. Ba^{2+} ions actively participate in a topochemical or topotactical reaction in the $BaCl_2 - KCl$ system whereby Ba^{2+} ions are incorporated in the bulk material.

For the molten-salt synthesis, salts were chosen which did not undergo a topotactical reaction and which did not react with the barium-titanium precursor. Salts with sufficient aqueous solubility were chosen so as to remove the salts much easier by washing. Also, the melting temperature of the eutectic salt mixture should be high enough to ensure full crystallization of barium titanate. In this regard, barium titanate was prepared in a $NaCl - KCl$ eutectic salt mixture. Rather than using separate barium and titanium precursors the barium-titanium precursor described in 2.1 was used for the molten-salt synthesis of $BaTiO_3$. By using a barium-titanium precursor whereby the constituent atoms were mixed at a quasi atomic level, the homogeneity of the end-product was aimed.[38]

For the molten-salt synthesis the barium-titanium precursor material was mixed in ethanol (99.9%, Merck). Afterwards, a 1:1 molar ratio of NaCl (99.5%, Janssen Chimica) - KCl (99%, Merck) (1:1 molar ratio) was prepared. The $NaCl - KCl$ salt mixture, with a melting temperature of 657°C, was added to the barium-titanium precursor/ethanol mixture by a 1:1 ratio, relative to the precursor's dry weight. After magnetically stirring of the salt–precursor mixture overnight, the salt–precursor mixture was transferred to a platinum crucible. The platinum crucible with its content was then heated to 70°C for 1 h in a furnace to fully evaporate the ethanol. Afterwards, the furnace was heated to 1080°C with a heating rate of 5°C min^{-1} and the furnace was held at 1080°C for 1 h. The furnace was then slowly cooled (furnace cooling) to room temperature. The mixture was then washed with warm demineralized water 5 times by centrifugation in order to remove NaCl and KCl from the end-product. The median particle-size of the molten-salt prepared $BaTiO_3$ was 0.93 µm (see Fig. 1b).

2.4. Colloidally processing of $BaTiO_3$

Colloidal dispersions of the hydrothermally prepared $BaTiO_3$ powder (see 2.2) for slip cast experiments were

prepared as follows. Powders were dispersed in demineralized water with 5 and 15 vol% solid loading. After addition of 0.5 wt% Darvan-C-N dispersant (R.T. Vanderbilt Company, Inc), relative to dry $BaTiO_3$ powder, the mixture was ultrasonicated for 3 minutes and the pH of the dispersion was adjusted to 10.5 with NH_4OH (28-30%, Acros). After stirring the colloidal dispersion for 1 h, the dispersion was slip casted in a gypsum mold and placed at the center of a 9.4 T magnet with the slip casting direction perpendicular to the magnetic field (B) direction.

The magnetic susceptibility of the c-axis for tetragonal $BaTiO_3$ was presumed to be smaller than for the a,b-axes ($\chi_{a,b} > \chi_c$ with $\chi < 0$ and $|\chi| \ll 1$). Hence, the slip casts were rotated (see Fig. 2) to ensure orientation of the c-axis normal to the magnetic field B.[39,40]

Once the colloidal dispersion settled, the green slip casts were calcinated first with a heating rate of 1.7°C min^{-1} to 1100°C and a dwell time of 4 h at 1100°C. The furnace was then cooled to room temperature with a cooling rate of 3°C min^{-1}. Next, the calcinated casts were sintered in a separate furnace with a heating rate of 1.7°C min^{-1} to 1400°C or 1500°C and a dwell time of 2 h at the final temperature. Finally, the furnace was cooled to room temperature by 3°C min^{-1}.

The surface parallel to the magnetic field B was analyzed by the X-ray diffraction (XRD) method. There are several ways to examine the texture degree of materials by XRD. One such method is the texture coefficient whereby individual line intensities are compared to line intensities of the reference sample or standard.[41] This is a semi-quantitative method that gives the relative line intensities of indivual (hkl) planes. Another semi-quantitave method is the Lotgering factor or the orientation factor[6,42] whereby a selected family of planes are compared to family of planes from a reference sample. The resulting value varies from 0 to 1 whereby 0 infers a randomly oriented sample and 1 a fully oriented sample. Since the <001> direction is of interest for $BaTiO_3$ ceramics, and to be consistent with literature, the {001} planes will be investigated by the orientation factor method. The orientation factor f was determined according to eq.(4) and eq.(5) in the 20-50° 2θ range.

$$f = \frac{P - P_0}{1 - P_0} \qquad (4)$$

$$\text{with} \quad P = \frac{\Sigma\, I\{001\} + \Sigma\, I\{100\}}{\Sigma\, I\{hkl\}} \qquad (5)$$

where the subscript 0 in eq.(4) denotes the random sample, i.e. the hydrothermal $BaTiO_3$ powder.

Densities of the sintered casts were determined by Archimedes' principle by immersion in water and expressed relatively to the theoretical density (TD) of $BaTiO_3$ (6.02 g cm^{-3}). Scanning electron microscopy (SEM) observations were made to study the microstructure of the sintered casts.

2.5. Instrumental

SEM images were obtained on a JEOL JSM-5510 (Oxford Inca software) with an acceleration voltage of 20 keV.

Electron probe micro-analysis (EPMA) measurements were conducted on a JEOL JXA-733 superprobe with an acceleration voltage of 25 kV and wire current of 0.1 nA. The XRD patterns were collected for 20 s in the 0 – 10 keV range.

Transmission electron microscopy (TEM) and selected area electron diffraction (SAED) measurements were conducted on a FEI Tecnai G2 equipment. Samples were prepared by crushing the powder in ethanol and depositing it on a holey carbon grid.

XRD patterns of powders were collected with a PANalytical X'Pert PRO MPD diffractometer (X'Pert Data Collector software) using a Ni-monochromator and Cu-Kα radiation (λ = 0.1540598 nm). The tube voltage and the tube current were set at 40 kV and 40 mA, respectively. The scan step size was 0.04° 2θ with 4 seconds per step. X-ray diffraction patterns of the sintered casts were collected with a PANalytical X'Pert PRO MPD diffractometer using a curved graphite-monochromator and Cu-Kα radiation. The tube voltage and the tube current were set at 40 kV and 40 mA, respectively. The scan step size was 0.04° 2θ with 4 seconds per step.

Densities of the sintered slip casts were determined in water by Archimedes' principle.

Particle-size distributions were determined with a CPS Disc Centrifuge DC24000 equipment. All analyses were run against a known calibration standard (diameter= 0.377 µm, density= 1.385 g ml^{-1}). Particle-size data were analyzed by means of the Disc Centrifuge Control System software.

Slip cast experiments were conducted in an MRI equipment from Bruker (Biospec 9.4T). The field strength of the Biospec horizontal magnet was 9.4 tesla (T) and the magnet's horizontal clear bore was 200 mm. The actively shielded gradient-insert had an inner diameter of 121 mm.

3. Results and Discussion

The XRDs and SEMs of the barium-titanium precursor, the hydrothermally derived $BaTiO_3$ powder and the MSS prepared $BaTiO_3$ are given in Fig. 3. The XRD of the barium-titanium precursor shows the amorphous character of the precursor material. EPMA gave a barium to titanium ratio of unity. Phase-pure $BaTiO_3$ (ICDD card #01-074-2491) was observed in XRD for the molten-salt and hydrothermally derived powders. TEM and SAED patterns of MSS synthesized $BaTiO_3$ particles are shown in Fig. 4. SAED measurements were done specifically on two particles with incompletely grown habit planes in order to determine the various facets. SAED of particles a and b were taken along the, respectively, [101] and [001] zone axis (see Fig. 4(a2) and Fig. 4(b2)). SAED patterns were fitted to the tetragonal crystal structure and the different habit-planes of particles a and b were deduced from the electron diffraction patterns. Results are shown in figure Fig. 4(a3) and Fig. 4(b3). The basal planes of particles a and b were thus, respectively, {101} and {001} oriented.

The magnetization energy ($\Delta E = |E_{a,b} - E_c|$) can be calculated from eq.(1), assuming that the $BaTiO_3$ powder consists of single-crystalline, non-agglomerated and freely rotating particles in the colloidal dispersion. However, very little is known about the $\chi_{a,b}$ and χ_c values of barium titanate, but $\Delta\chi = |\chi_{a,b} - \chi_c|$ values for $BaTiO_3$ were measured and vary depending on the type of material measured.[43–46]

Furthermore, ΔE should be greater than the particle's thermal energy ($E_{thermal} = k_B T$) at all times to be able to align in the magnetic field.[13] For example, ΔE was calculated as 9.4 x 10^{-18} J for fixed values of T = 300 K, B = 9.4 T and $\Delta\chi = 10^{-7}$ (dimensionless, volume susceptibility). This value for ΔE is larger than the particle's thermal energy ($E_{thermal} = 4.14 \times 10^{-21}$ J). Hence, if $BaTiO_3$ has a $\Delta\chi$ value of ~10^{-7} it would be eligible for magnetic alignment experiments.[13]

5 vol% and 15 vol% dispersions of hydrothermal $BaTiO_3$ (with and without templates) with 0.5 wt%

Darvan-C-N were processed by slip casting inside a 9.4 T magnet. The sintered casts with the different heating conditions are depicted in Table 1.

The XRDs of the 5 vol% and 15 vol% sintered casts (with and without templates) are shown in Fig. 5. Fig. 5a is the hydrothermal powder which was used as reference (i.e., random orientation) for the calculation of the orientation factor (f).

Sintered casts were also analyzed by SEM. The top surfaces (parallel to the magnetic field B) and the side surfaces of the sintered casts are depicted in Fig. 6. Grain-sizes were analyzed by measuring the average diameter of about 50 grains on each surface. The top-to-side grain-size ratios were low and inferred spherical grains.

The addition of templates (BT5 + t) resulted in a larger grain-size. This larger grain-size was the result of the abnormal grain-growth (AGG) mechanism whereby template particles grew discontinuously at the expense of matrix particles. The abnormal grains formed in the initial stage of AGG can grow without impingement over a long period of time to relatively big grains. AGG stops at a point where further growth is no longer thermodynamically favorable.[47] By adding templates, the big template particles acted as starting grains for AGG. The increase of the orientation factor (from 0.38 to 0.67) showed that grain-growth occurred along the template's habit planes which were {001} and {101} oriented (see Fig. 4). The mild decrease in the relative density was the result of templates impinging on each other during the grain-growth process. For the 15 vol% sample (BT15) the average grain-size was decreased by more than 50% and the orientation factor increased only mildly (0.44). The relatively high solid loading was thought to impinge grain-growth resulting in a porous sintered cast with a lower relative density. When template particles were added to the 15 vol% cast (BT15 + t) the average grain-size and the orientation factor decreased considerably. The grain-size after sintering was controlled by the number and distribution of starting grains (i.e., templates) at the initial stage of AGG.[47] AGG in the templated 15 vol% cast is significantly reduced since, relatively speaking, more big template particles were present for sample (BT15 + t). Consequently, the orientation factor (0.29) was not fully developed and remained relatively low. Also, the strong impingement effect due to the higher solid loading and AGG of template particles decreased the relative density of sample BT15 + t to 62.1%.

The effect of a higher sintering temperature, a slower heating rate, and sintering without a calcination step was also studied. The XRDs are depicted in Fig. 7 and the SEM images are given in Fig. 8.

Sintering at 1500°C (BT5-1500) seems to have a positive effect on the orientation factor (0.49) in comparison to BT5. Barium titanate alignment in a strong magnetic field was reported by Özen et al[6]. However, $BaTiO_3$ samples were sintered at 1400°C. Here, it was observed that sintering at 1500°C can improve texture of $BaTiO_3$. Vriami et al.[4] also reported an improvement of the orientation factor for $BaTiO_3$ (prepared by the same synthesis route as described in 2.1 and 2.2) aligned by electrophoretic deposition in a 17.4 T vertical magnet and sintered at 1500°C. The slip casted sample showed a maximum in the orientation factor at 1450°C and a mild decrease at 1500°C. In any case, the orientation factor of the slip casted $BaTiO_3$ samples were reported to be increased at and above 1450°C in comparison to the slip casted sample which was sintered at 1400°C.[4] Also, it is noteworthy to mention that $BaTiO_3$ is hexagonal at 1500°C, as opposed to cubic at 130°C □ ~1420°C.[26] The average grain-size was also increased (see Table 1) and a mild decrease of the relative density was measured. Elimination of the calcination step by directly sintering to 1400°C (BT5-1400) did not have a positive effect on the orientation factor. A decrease in f was calculated for the latter (0.31). SEM images of BT5-1400 revealed a rather coalesced cast with no distinguishable grain-boundaries. The elimination of the calcination step clearly degraded the sample's integrity due to uncontrolled combustion of the organic matter (dispersant) and resulted in a highly porous cast after sintering with a low relative density. A slower heating rate (0.34°C min^{-1}) resulted in an increase of f to 0.70 (BT5-s1400). A slow heating rate most likely decreased stresses in the slip cast caused by grain-growth and the crystal phase transformation of $BaTiO_3$ (i.e., from tetragonal to cubic and vice versa) resulting in a relatively high orientation factor. The controlled grain-growth also resulted in a relatively low average grain-size (21.5 µm / 24 µm) for BT5-s1400 and a relatively high density (see Table 1).

4. Conclusions

Hydrothermally derived $BaTiO_3$ powder was slip casted in a 9.4 T magnet and molten-salt synthesized (MSS) $BaTiO_3$ was used as templates. It was seen that large particles with defined habit planes can serve as templates (i.e., MSS $BaTiO_3$) for the templated grain-growth of matrix particles (i.e., hydrothermal $BaTiO_3$).

The abnormal grain-growth (AGG) is an important factor to consider when working with templates with large dimensions. Addition of templates will increase the number of starting grains. Consequently, the grains grow abnormally large to a point where further growth is no longer thermodynamically favorable. AGG usually results in a porous cast after sintering with a decreased relative density. Templates have a positive effect on the orientation factor at low solid loadings, but AGG is extensive and result in relatively high grain-sizes. For higher solid loadings impingement effects predominate and lead to misorientation of particles. Hence, a low orientation factor is obtained after sintering.

The orientation factor can be increased by increasing the sintering temperature and applying a slow heating rate when sintering the slip cast. In the latter case, a slow heating will decrease stresses in the cast due to organic matter combustion and crystal phase transformations.

Acknowledgements

This work was financially supported by the Flemish Institute for the Promotion of Scientific Technological Research in Industry (IWT) under contract SBO-PROMAG (60056). The research was also performed within the framework of a GOA-BOF project supported by the University of Antwerp. The authors want to thank Prof. A. Van Der Linden for providing a 9.4 T magnet.

References

[1] W. Chen, Y. Kinemuchi, T. Tamura, K. Miwa, K. Watari, Fabrication of textured ferroelectric ceramics by magnetic alignment via gelcasting, J. Eur. Ceram. Soc. 27 (2007) 655–661. doi:10.1016/j.jeurceramsoc.2006.04.087.

[2] A. Szudarska, T. Mizerski, Y. Sakka, T.S. Suzuki, M. Szafran, Fabrication of textured alumina by magnetic alignment via gelcasting based on low-toxic system, J. Eur. Ceram. Soc. 34 (2014) 3841–3848. doi:10.1016/j.jeurceramsoc.2014.05.017.

[3] Z. Yang, J. Yu, K. Deng, L. Lan, H. Wang, Z. Ren, et al., Fabrication of textured Si_3N_4 ceramics with β-Si_3N_4 powders as raw material by gel-casting under strong magnetic field, Mater. Lett. 135 (2014) 218–221. doi:10.1016/j.matlet.2014.07.038.

[4] D. Vriami, E. Beaugnon, P. Cool, J. Vleugels, O. Van der Biest, Hydrothermally synthesized $BaTiO_3$ textured in a strong magnetic field, Ceram. Int. 41 (2015) 5397–5402. doi:10.1016/j.ceramint.2014.12.104.

[5] S. Wada, T. Kita, I. Fujii, K. Nakashima, T. Takei, N. Kumada, et al., Preparation of Barium Titanate Grain-Oriented Ceramics by Electrophoresis Deposition Method under High Magnetic Field Using Single-Domain Nanoparticles, Key Eng. Mater. 582 (2013) 27–31. doi:10.4028/www.scientific.net/KEM.582.27.

[6] M. Özen, M. Mertens, M. Schroeven, F. Snijkers, P. Cool, Preparation of barium titanate powders and colloidal processing in a strong (9.4T) magnetic field, Mater. Lett. 67 (2012) 154–157. doi:10.1016/j.matlet.2011.09.071.

[7] X.W. Zhu, Y. Sakka, Y. Zhou, K. Hirao, K. Itatani, A strategy for fabricating textured silicon nitride with enhanced thermal conductivity, J. Eur. Ceram. Soc. 34 (2014) 2585–2589. doi:10.1016/j.jeurceramsoc.2014.01.025.

[8] Z. Gao, T.S. Suzuki, S. Grasso, Y. Sakka, M.J. Reece, Highly anisotropic single crystal-like $La_2Ti_2O_7$ ceramic produced by combined magnetic field alignment and templated grain growth, J. Eur. Ceram. Soc. 35 (2015) 1771–1776. doi:10.1016/j.jeurceramsoc.2014.12.003.

[9] T. Hagio, K. Yamauchi, T. Kohama, T. Matsuzaki, K. Iwai, Beta tricalcium phosphate ceramics with controlled crystal orientation fabricated by application of external magnetic field during the slip casting process, Mater. Sci. Eng. C. 33 (2013) 2967–2970. doi:10.1016/j.msec.2013.03.024.

[10] T. Sato, T. Kimura, Preparation of <111>-textured $BaTiO_3$ ceramics by templated grain growth method using novel template particles, Ceram. Int. 34 (2008) 757–760. doi:10.1016/j.ceramint.2007.09.021.

[11] S. Wada, K. Takeda, T. Muraishi, H. Kakemoto, T. Tsurumi, T. Kimura, Preparation of [110] Grain Oriented Barium Titanate Ceramics by Templated Grain Growth Method and Their Piezoelectric Properties, Jpn. J. Appl. Phys. 46 (2007) 7039–7043. doi:10.1143/JJAP.46.7039.

[12] T.S. Suzuki, Y. Miwa, S. Kawada, M. Kimura, T. Uchikoshi, Y. Sakka, Two-Dimensional Orientation in $Bi_4Ti_3O_{12}$ Prepared Using Platelet Particles and a Magnetic Field, J. Am. Ceram. Soc. 96 (2013) 1085–1089. doi:10.1111/jace.12238.

[13] Y. Sakka, T.S. Suzuki, Textured development of feeble magnetic ceramics by colloidal processing under high magnetic field, J. Ceram. Soc. Jpn. 113 (2005) 26–36. doi:10.2109/jcersj.113.26.

[14] H. Morikawa, K. Sassa, S. Asai, Control of precipitating phase alignment and crystal orientation by imposition of a high magnetic field, Mater. Trans. Jim. 39 (1998) 814–818. doi:10.2320/matertrans1989.39.814.

[15] S. Asai, K. Sassa, M. Tahashi, Crystal orientation of non-magnetic materials by imposition of a high magnetic field, Sci. Technol. Adv. Mater. 4 (2003) 455–460. doi:10.1016/j.stam.2003.07.001.

[16] J.C. Burfoot, Ferroelectrics: an introduction to the physical principles, Van Nostrand, 1967.

[17] E. Lines, A.M. Glass, Principles and Applications of Ferroelectrics and Related Materials, OUP Oxford, 1977.

[18] B. Li, W. Shang, Z. Hu, N. Zhang, Template-free fabrication of pure single-crystalline $BaTiO_3$ nano-wires by molten salt synthesis technique, Ceram. Int. 40 (2014) 73–80. doi:10.1016/j.ceramint.2013.05.105.

[19] N. Kumada, A. Miura, T. Takei, I.B. Adilina, S. Shimazu, Low temperature synthesis of $ATiO_3$ (A: Mg, Ca, Sr, Ba) by using molten salt, J. Ceram. Soc. Jpn. 121 (2013) 74–79. doi:10.2109/jcersj2.121.74.

[20] Y. Zhang, L. Wang, D. Xue, Molten salt route of well dispersive barium titanate nanoparticles, Powder Technol. 217 (2012) 629–633. doi:10.1016/j.powtec.2011.11.043.

[21] Y. Kan, X. Jin, P. Wang, Y. Li, Y.-B. Cheng, D. Yan, Anisotropic grain growth of $Bi_4Ti_3O_{12}$ in molten salt fluxes, Mater. Res. Bull. 38 (2003) 567–576. doi:10.1016/S0025-5408(03)00029-1.

[22] K.H. Yoon, Y.S. Cho, D.H. Kang, Molten salt synthesis of lead-based relaxors, J. Mater. Sci. 33 (1998) 2977–2984. doi:10.1023/A:1004310931643.

[23] K. Byrappa, M. Yoshimura, Handbook of hydrothermal technology, William Andrew, Norwich, N.Y., 2012.

[24] M. Yoshimura, K. Byrappa, Hydrothermal processing of materials: past, present and future, J. Mater. Sci. 43 (2008) 2085–2103. doi:10.1007/s10853-007-1853-x.

[25] J. Moon, M.L. Carasso, H.G. Krarup, J.A. Kerchner, J.H. Adair, Particle-shape control and formation mechanisms of hydrothermally derived lead titanate, J. Mater. Res. 14 (1999) 866–875. doi:10.1557/JMR.1999.0116.

[26] S. Lee, C.A. Randall, Z.-K. Liu, Modified Phase Diagram for the Barium Oxide-Titanium Dioxide System for the

Ferroelectric Barium Titanate, J. Am. Ceram. Soc. 90 (2007) 2589–2594. doi:10.1111/j.1551-2916.2007.01794.x.

[27] M. Özen, M. Mertens, J. Luyten, F. Snijkers, H. D'Hondt, P. Cool, Hydrothermal synthesis of carbonate-free submicron-sized barium titanate from an amorphous precursor: Synthesis and characterization, Ceram. Int. 38 (2012) 619–625. doi:10.1016/j.ceramint.2011.07.051.

[28] G. Schwarzenbach, J. Muehlebach, K. Mueller, Peroxo complexes of titanium, Inorg. Chem. 9 (1970) 2381–2390. doi:10.1021/ic50093a001.

[29] J. Livage, M. Henry, C. Sanchez, Sol-gel chemistry of transition metal oxides, Prog. Solid State Chem. 18 (1988) 259–341. doi:10.1016/0079-6786(88)90005-2.

[30] J. Adam, G. Klein, T. Lehnert, Hydroxyl Content of $BaTiO_3$ Nanoparticles with Varied Size, J. Am. Ceram. Soc. 96 (2013) 2987–2993. doi:10.1111/jace.12404.

[31] D. Liu, Y. Yan, H. Zhou, Synthesis of Micron-Scale Platelet $BaTiO_3$, J. Am. Ceram. Soc. 90 (2007) 1323–1326. doi:10.1111/j.1551-2916.2007.01525.x.

[32] H. Liu, C. Hu, Z.L. Wang, Composite-Hydroxide-Mediated Approach for the Synthesis of Nanostructures of Complex Functional-Oxides, Nano Lett. 6 (2006) 1535–1540. doi:10.1021/nl061253e.

[33] D.D. Jayaseelan, S. Zhang, S. Hashimoto, W.E. Lee, Template formation of magnesium aluminate ($MgAl_2O_4$) spinel microplatelets in molten salt, J. Eur. Ceram. Soc. 27 (2007) 4745–4749. doi:10.1016/j.jeurceramsoc.2007.03.027.

[34] D. Lv, R. Zuo, S. Su, Processing and Morphology of (111) $BaTiO_3$ Crystal Platelets by a Two-Step Molten Salt Method, J. Am. Ceram. Soc. 95 (2012) 1838–1842. doi:10.1111/j.1551-2916.2012.05124.x.

[35] S. Su, R. Zuo, D. Lv, J. Fu, Synthesis and characterization of (001) oriented $BaTiO_3$ platelets through a topochemical conversion, Powder Technol. 217 (2012) 11–15. doi:10.1016/j.powtec.2011.09.045.

[36] K.-H. Park, S.-I. Gu, H.-S. Shin, D.-H. Yeo, H.-S. Kim, G.-H. Ha, Effect of Water in the Synthesis of Nano $BaTiO_3$ Particle Using Potassium Hydroxide, Asian J. Chem. 25 (2013) 5615–5618.

[37] C.H. Lee, H.S. Shin, D.H. Yeo, G.H. Ha, S. Nahm, Synthesis Mechanism of Nano $BaTiO_3$ Particles at Low Temperature by Molten Salt Method, Asian J. Chem. 26 (2014) 4125–4127. doi:10.14233/ajchem.2014.17730.

[38] A.R. West, Solid State Chemistry and its Applications, 2nd ed., John Wiley & Sons, New York, 2014.

[39] X.W. Zhu, Y. Sakka, T.S. Suzuki, T. Uchikoshi, S. Kikkawa, The c-axis texturing of seeded Si_3N_4 with β-Si_3N_4 whiskers by slip casting in a rotating magnetic field, Acta Mater. 58 (2010) 146–161. doi:10.1016/j.actamat.2009.08.064.

[40] S. Tanaka, A. Makiya, Z. Kato, K. Uematsu, c-axis oriented ZnO formed in a rotating magnetic field with various rotation speeds, J. Eur. Ceram. Soc. 29 (2009) 955–959. doi:10.1016/j.jeurceramsoc.2008.07.025.

[41] D. Jadsadapattarakul, C. Euvananont, C. Thanachayanont, J. Nukeaw, T. Sooknoi, Tin oxide thin films deposited by ultrasonic spray pyrolysis, Ceram. Int. 34 (2008) 1051 – 1054. doi:http://dx.doi.org/10.1016/j.ceramint.2007.09.096.

[42] F.K. Lotgering, Topotactical reactions with ferrimagnetic oxides having hexagonal crystal structures—I, J. Inorg. Nucl. Chem. 9 (1959) 113–123. doi:10.1016/0022-1902(59)80070-1.

[43] J. Hwang, T. Kolodiazhnyi, J. Yang, M. Couillard, Doping and temperature-dependent optical properties of oxygen-reduced $BaTiO_{\{3-\delta\}}$, Phys. Rev. B. 82 (2010) 214109. doi:10.1103/PhysRevB.82.214109.

[44] M. Nasir Khan, H.-T. Kim, H. Minami, H. Uwe, Thermoelectric properties of niobium doped hexagonal barium titanate, Mater. Lett. 47 (2001) 95–101. doi:10.1016/S0167-577X(00)00229-9.

[45] T. Kolodiazhnyi, A. Belik, S. Wimbush, H. Haneda, Electrical and magnetic properties of hexagonal $BaTiO_{3-\delta}$, Phys. Rev. B. 77 (2008). doi:10.1103/PhysRevB.77.075103.

[46] R. Pązik, D. Kaczorowski, D. Hreniak, W. Stręk, W. Łojkowski, Synthesis, structure and magnetic properties of $BaTiO_3$ nanoceramics, Chem. Phys. Lett. 452 (2008) 144–147. doi:10.1016/j.cplett.2007.12.037.

[47] Y.-I. Jung, S.-Y. Choi, S.-J.L. Kang, Grain-Growth Behavior during Stepwise Sintering of Barium Titanate in Hydrogen Gas and Air, J. Am. Ceram. Soc. 86 (2003) 2228–2230. doi:10.1111/j.1151-2916.2003.tb03640.x.

Figure Captions

Fig. 1: Particle-size distributions of (a) the hydrothermally derived $BaTiO_3$: median weight: 0.48 µm (residual peak at ~0.035 µm), and (b) the MSS produced $BaTiO_3$: median weight 0.93 µm (peaks at 0.50 µm and 0.81 µm).

Fig. 2: Schematic view of slip cast experiments in the 9.4 T magnet. The slip slurry is cast into a gypsum mold which is rotating at the center of the magnet by a rotor (B = magnetic field).

Fig. 3: XRD and SEM of (a) the barium-titanium precursor, (b) the molten-salt and (c) the hydrothermally derived $BaTiO_3$. All diffraction lines in (b) and (c) belong to tetragonal $BaTiO_3$ phase (ICDD card #01-074-2491).

Fig. 4: TEM and SAED patterns of two $BaTiO_3$ particles prepared by the molten-salt method.

Fig. 5: XRD of (a) hydrothermal $BaTiO_3$ powder (reference), (b) BT5, (c) BT5 + t, (d) BT15, (e) BT15 + t. All diffraction lines belong to tetragonal $BaTiO_3$ phase (ICDD card #01-074-2491).

Fig. 6: SEM of sintered casts with top (above) and side (below) images: (a) BT5, (b) BT5 + t, (c) BT15, and (d) BT15 + t.

Fig. 7: XRD of (a) hydrothermal $BaTiO_3$ powder (reference), (b) BT5, (c) BT5-1500, (d) BT5-1400, (e) BT5-s1400. All diffraction lines belong to tetragonal $BaTiO_3$ phase (ICDD card #01-074-2491).

Fig. 8: SEM of sintered casts with top (above) and side (below) images: (a) BT5-1400, (b) BT5-1500, and (c) BT5-s1400.

Tables

Table 1: Solid loading, template concentration, orientation factor, relative density, and grain size of the sintered $BaTiO_3$ casts.

sample	solid loading (vol%)	template (t) loading (wt%)	orientation factor (f)	density sintered cast (% TD)	average grain size top / side surface (µm)
Powder	–	–	0	–	–
BT5	5	–	0.38	90.1	99.5 / 57
BT5 + t	5	20	0.67	89.4	145 / 116
BT15	15	–	0.44	87.9	40.5 / 43.5
BT15 + t	15	12	0.29	62.1	32 / 16.5
BT5-1400	5	–	0.31	87.2	–*
BT5-1500	5	–	0.49	89.5	111.5 / 99
BT5-s1400	5	–	0.70	92.7	21.5 / 24

* no clear grain boundaries observed